Density functional theory for hydrogen storage materials: successes and opportunities

2008 J. Phys.: Condens. Matter 20 064229

(http://iopscience.iop.org/0953-8984/20/6/064229)

IOP PUBLISHING JOURNAL OF PHYSICS: CONDENSED MATTER

J. Phys.: Condens. Matter **20** (2008) 064229 (11pp) doi:10.1088/0953-8984/20/6/064229

Density functional theory for hydrogen storage materials: successes and opportunities

L G Hector Jr and J F Herbst

General Motors R&D Center, 30500 Mound Road, Warren, MI 48090, USA

E-mail: Louis.Hector@gm.com

Received 26 October 2007
Published 24 January 2008
Online at stacks.iop.org/JPhysCM/20/064229

Abstract

Solid state systems for hydrogen storage continue to be the focus of considerable international research, driven to a large extent by technological demands, especially for mobile applications. Density functional theory (DFT) has become a valuable tool in this effort. It has greatly expanded our understanding of the properties of known hydrides, including electronic structure, hydrogen bonding character, enthalpy of formation, elastic behavior, and vibrational energetics. Moreover, DFT holds substantial promise for guiding the discovery of new materials. In this paper we discuss, within the context of results from our own work, some successes and a few shortcomings of state-of-the-art DFT as applied to hydrogen storage materials.

1. Introduction

As an energy carrier, hydrogen is a strong candidate among alternatives to hydrocarbon fuels, especially in the transportation sector. The driving force is the mounting concern for environmental issues such as global climate change and pollution as well as energy security. Hydrogen is attractive for several reasons. First, it is available in vast amounts as a component of water. Second, its reaction with oxygen yields only water vapor and heat and does not produce any greenhouse gases such as CO_2. This characteristic makes hydrogen fuel cells auspicious candidates to replace hydrocarbon-powered internal combustion engines. Third, the gravimetric energy density of H_2 is about three times that of petrol. The US Department of Energy (DOE) has set 2010 goals of 6 mass% and 45 g l^{-1} for a hydrogen storage system onboard a motor vehicle. Storing H_2 as a compressed gas is technically feasible; ∼4 mass% and ∼20 g l^{-1} capacities have been realized with high-pressure tanks. The volumetric density can be doubled with liquid H_2 storage, but a superinsulated cryogenic tank is required and boil-off generated by heat leaks is a major issue. Since many hydrides (e.g., $LaNi_5H_7$, MgH_2) feature volumetric hydrogen density greater than that of liquid H_2, solid hydrides are of great interest as hydrogen storage media. Neither the compressed or liquid options nor any material satisfies the DOE objectives at present. Substantial progress has been achieved on the materials front, and density functional theory (DFT) has become an increasingly valuable tool in this effort, as the large and expanding body of literature in the area makes abundantly clear. In our opinion there are specific technical issues that merit consideration, however, and here we draw attention to some of these in the context of our own work on DFT property predictions of hydrogen storage materials. Addressing these offers potential for enhancing the utility of DFT not only for deepening our knowledge of known materials but for guiding the discovery and development of new materials and mechanisms for hydrogen storage.

The paper is organized as follows. We first summarize our computed enthalpies of formation for the alkaline earth hydrides predicted within both the LDA and GGA. We then critically examine which of the two exchange–correlation functionals (ε_{xc}) leads to better agreement with experiment. We next address the important issue of crystal structure prediction with DFT by exploring the energetics of the Li amide/Li imide hydrogen storage reaction using four different Li_2NH (lithium imide) structures, only one of which has been confirmed by experiment. We also compute elasticity tensor components and investigate mechanical stability of the relevant solid phases over a range of applied pressures using the Born stability criteria. Predicted phonon spectra generated with the direct method along with a review of recently predicted decomposition reactions are then examined for the recently discovered ternary hydride $Li_4BN_3H_{10}$. Finally, predicted

vibrational properties of $LaCo_5$, the parent compound of $LaCo_5H_4$, are compared with experiment.

2. Computational details

All results reported here were obtained with the Vienna *ab initio* simulation package (VASP), which implements DFT [1] using a plane wave basis set [2, 3]. All-electron projector-augmented wave potentials [4, 5] were employed for the elemental constituents. The exchange–correlation part ε_{xc} of the density functional was treated within the local density approximation (LDA) of Ceperley–Alder [6] as parameterized by Perdew–Zunger [7] and within the GGA of Perdew and Wang (PW91) [8, 9] or Perdew–Burke–Ernzerhof (PBE) [10] in conjunction with the interpolation formula of Vosko *et al* [11]. Lattice constants and nuclear coordinates were relaxed simultaneously at least twice for each solid. This allowed for adaptation of the numerical grids to changed lattice parameters. The energy of the H_2 molecule was calculated in an orthorhombic box large enough to ensure isolation. In all cases the electronic total energy was converged to 10^{-6} eV/cell and the force components on each atom relaxed to less than 10^{-3} eV Å^{-1}. Phonon spectra for the solids and the vibrational frequency of the H_2 molecule were computed with the direct method [12] using VASP as the computational engine.

3. Alkaline earth metals and hydrides

From the hydrogen storage perspective MgH_2 is the most interesting of these materials because of its 7.6 mass% hydrogen content. A large enthalpy of hydride formation (-76 kJ mol^{-1} H_2) and slow sorption kinetics obviate technological viability of the pure material, stimulating considerable work on destabilizing additives [13–17] and reactions with other hydrides [18]. Since the properties of the entire class are reasonably well known, the alkaline earth metals and hydrides offer a fertile test bed for systematic theoretical work [19]. For the present discussion we focus on formation enthalpies computed with both the LDA and GGA (PW91).

We express the enthalpy of formation ΔH_T of a metal from its constituent atoms at temperature T as

$$\begin{aligned}\Delta H_T &= (E+pV)_{\text{metal}} - (E+pV)_{\text{atom}} \\ &\approx (-|E_{\text{atom}}| + E_{\text{el}} + E_{\text{ZPE}} + E_{\text{ph}}) - (-|E_{\text{atom}}| + \tfrac{5}{2}kT) \\ &= E_{\text{el}} + E_{\text{ZPE}} + (E_{\text{ph}} - \tfrac{5}{2}kT) \equiv E_{\text{el}} + E_{\text{ZPE}} + \delta\Delta H_T.\end{aligned} \tag{1}$$

E_{atom} represents the total energy of the atom, and E_{el} is the VASP-optimized total energy of the metal with respect to $|E_{\text{atom}}|$. $E_{\text{ZPE}} = \frac{1}{2}\sum_{\vec{q}} \hbar\omega_{\vec{q}}$ is the zero-point energy (ZPE) of the metal in terms of the phonon frequencies $\omega_{\vec{q}}$; and $E_{\text{ph}} = \sum_{\vec{q}} \hbar\,\omega_{\vec{q}} n(\omega_{\vec{q}})$, $n(\omega) = (\mathrm{e}^{\hbar\omega/kT} - 1)^{-1}$, is the phonon energy of the metal at T (without the ZPE). The $\frac{5}{2}kT$ term is the sum of the translational energy $\frac{3}{2}kT$ and $pV = kT$ for the atom assuming the ideal gas law. We neglect pV for the metal since the small molar volume makes pV insignificant at $p = 1$ bar. The alkaline earth atoms are all characterized by

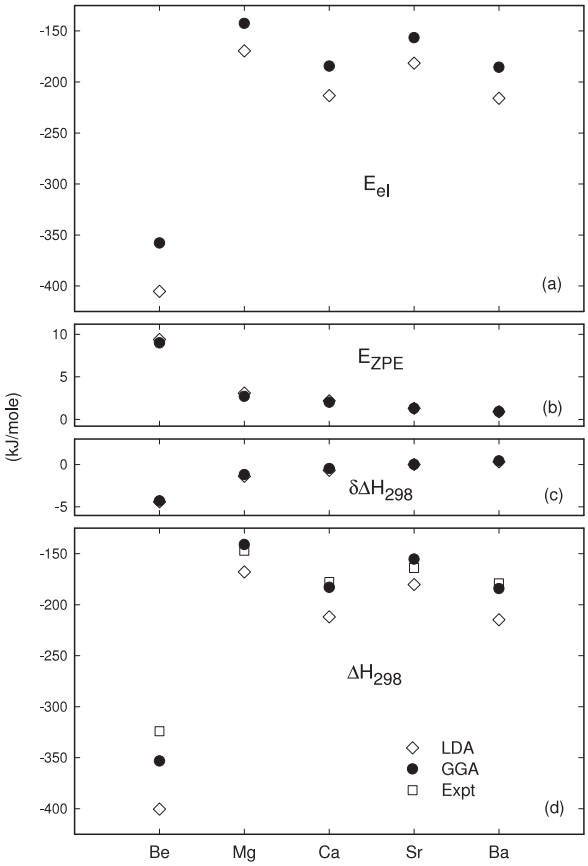

Figure 1. Components E_{el} (a), E_{ZPE} (b), and $\delta\Delta H_{298}$ (c) of the room temperature enthalpy of formation ΔH_{298} with respect to the atomic state (d) of the alkaline earth metals (cf equation (1)) in the LDA and GGA (PW91), and experimental values (d).

$^1S_0$ ground states and the metals are all nonmagnetic, so that no spin polarization terms enter. The $T = 0$ enthalpy of formation with respect to the atomic state is $\Delta H_0 \equiv E_{\text{el}} + E_{\text{ZPE}}$ and is the negative of the cohesive energy; $\delta\Delta H_T \equiv E_{\text{ph}} - \frac{5}{2}kT$ is the change in enthalpy from $T = 0$ to T. Figure 1 displays ΔH_{298} and its components for the alkaline earth metals obtained in both the LDA and GGA.

In analogy with equation (1) the enthalpy of formation of the hydrides with respect to the elemental metals and H_2 can be written as

$$\Delta H_T = \Delta H_{\text{el}} + \Delta H_{\text{ZPE}} + \delta\Delta H_T. \tag{2}$$

For MgH_2 as an example we have

$$\Delta H_{\text{el}}(\text{MgH}_2) = E_{\text{el}}(\text{MgH}_2) - E_{\text{el}}(\text{Mg}) - E_{\text{el}}(\text{H}_2), \tag{3}$$

$$\Delta H_{\text{ZPE}}(\text{MgH}_2) = E_{\text{ZPE}}(\text{MgH}_2) - E_{\text{ZPE}}(Mg) - E_{\text{ZPE}}(\text{H}_2), \tag{4}$$

and

$$\begin{aligned}&\delta\Delta H_T(\text{MgH}_2) \\ &\quad = E_{\text{ph}}(\text{MgH}_2) - E_{\text{ph}}(Mg) - \left[\tfrac{7}{2}kT + E_{\text{vib}}(\text{H}_2)\right].\end{aligned} \tag{5}$$

$E_{\text{vib}}(\text{H}_2) = \hbar\omega_0 n(\omega_0)$ is the vibrational energy of the H_2 molecule, and $\frac{7}{2}kT$ is the sum of its translational, pV, and

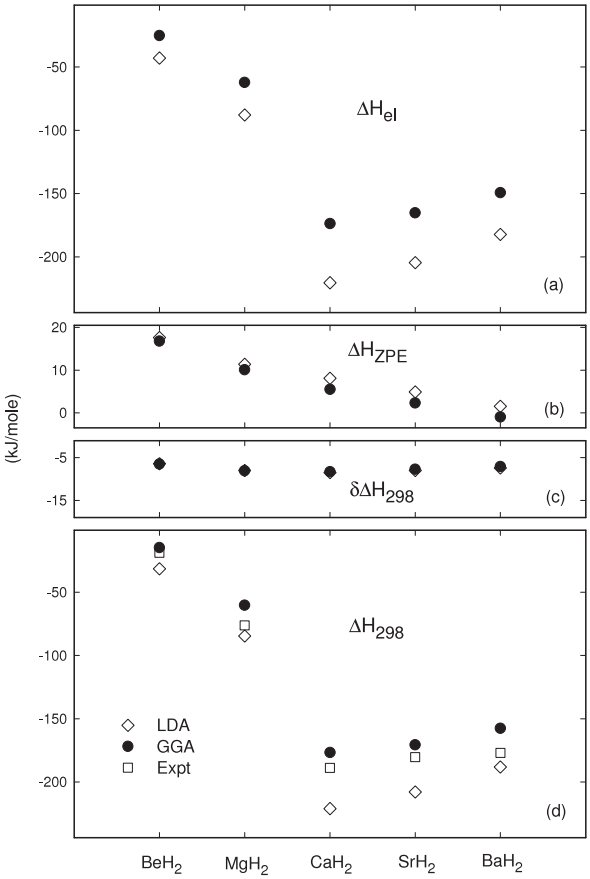

Figure 2. Components $\Delta H_{\rm el}$ (a), $\Delta H_{\rm ZPE}$ (b), and $\delta\Delta H_{298}$ (c) of the room temperature enthalpy of formation ΔH_{298} (d) of the alkaline earth hydrides (cf equations (2)–(5)) in the LDA and GGA (PW91), and experimental values (d).

rotational (kT) energies. $\Delta H_0 = \Delta H_{\rm el} + \Delta H_{\rm ZPE}$ is the zero temperature formation enthalpy. ΔH_{298} and its components for the alkaline earth hydrides are presented in figure 2.

It is evident that $E_{\rm el}$ in figure 1(a) and $\Delta H_{\rm el}$ in figure 2(a) are significantly different in the LDA and GGA. Our $\Delta H_{\rm el}$ in the GGA for the hydrides are in good agreement with the GGA calculations of Wolverton *et al* [20], while the LDA values depart more widely from the LDA work of Smithson *et al* [21]. The disparities are likely due to our use of PAW potentials here versus ultrasoft pseudopotentials in [20] and [21]. In contrast, we see from figures 1(b), (c) and 2(b), (c) that the ZPE and $\delta\Delta H_{298}$ components are small compared to the electronic terms and are nearly the same in the LDA and GGA. From figure 1(d) it is clear that ΔH_{298} calculated in the GGA is in more favorable agreement with experiment than the LDA results for all the metals. The same is true for the hydrides (figure 2) with the conspicuous exception of MgH_2, unfortunately the material of most interest technologically, for which the LDA provides a more accurate ΔH_{298}. This circumstance makes the choice of $\varepsilon_{\rm xc}$ for Mg-containing systems unclear. At present the results of figure 2 suggest a pragmatic, if not completely satisfying, approach: the LDA and GGA enthalpies bound the experimental values, so that calculation of both for a crystalline material for which measurements are not available can provide a reasonably reliable indication of thermodynamic stability.

4. Li amide/Li imide hydrogen storage reaction

4.1. Background

Spurred by the initial work of Chen *et al* [22], the reaction

$$\mathrm{LiNH_2 + LiH \leftrightarrow Li_2NH + H_2} \qquad (6)$$

has attracted substantial interest as a potential mechanism for hydrogen storage [23–26]. This system is especially noteworthy since it involves reaction of two stable compounds (lithium amide, $LiNH_2$, and LiH) to yield another stable compound (lithium imide, Li_2NH) and H_2 gas, rather than release of H_2 from a single parent phase. H_2 evolution initiates at ∼150 °C, lower than for either $LiNH_2$ (∼200 °C) or LiH (∼550 °C) alone [23], and the theoretical 6.5 mass% H_2 capacity is substantial. Technological interest would be enhanced, however, if the temperature $T \sim 280\,^{\circ}$C at which the hydrogen plateau pressure is $p \sim 1$ bar [22, 26] could be decreased. Prospects for doing so will be bolstered by further understanding of the fundamental properties of reaction (6). The crystal structures of $LiNH_2$ and LiH have been established for some time, and an accurate orthorhombic ($Ima2$) structure for Li_2NH has recently been determined [27]. Calculations of the electronic structure, enthalpies of formation, and vibrational properties of the constituents have been reported in [28]. Low temperature $Pnma$ [29] and $Pbca$ [30] Li_2NH structures were subsequently predicted by theoretical means. While intriguing, these structures have yet to receive experimental confirmation.

Using the hardest GGA (PBE [10]) PAW potentials in VASP, we compute the elastic constants for each solid state constituent of equation (6) and examine elastic stability under pressure. While in general the elastic constants dictate the speed of sound in a material [31] and are important to studies of dislocations [32] and structural transformations [33], they can be of specific value for hydrides. For example, Bereznitsky *et al* [34] have emphasized that the elastic constants can in some cases correlate with hydrogen sorption properties and can be useful in assessing H–H interaction energies and the deformation energy associated with hydride precipitation. We also compare the computed 298 K heats of formation for several Li_2NH structures as a means to explore some important questions about DFT energetics of these structures and the ultimate need for experimental corroboration. The plane wave cutoff energy was at least 900 eV in all cases, and we utilized **k**-meshes having 186, 280, and 64 **k**-points in the irreducible Brillouin zones of $LiNH_2$, LiH, and Li_2NH, respectively.

4.2. Crystal structures

For LiH the fcc ($Fm\bar{3}m$) structure in [35] was used, while [36, 37] supplied the necessary structural information for body-centered tetragonal $LiNH_2$. Balogh *et al* [27] have found that neutron powder diffraction data on the low temperature phase of deuterated Li_2NH can be represented

equally accurately by an fcc structure with partially occupied Li sites or by a fully occupied orthorhombic ($Ima2$) structure; here we choose the $Ima2$ representation since it eliminates the need to construct large supercells required to adequately treat partial occupancy [28]. Although predicted by other theoretical means, the $Pnma$ Li_2NH structure in [29] is readily constructed from SrNH (ICSD#410664) [38] by replacing Sr with Li and populating the cell with Li at additional 4c sites. This illustrates one means of deriving hypothetical structures from database searches.

4.3. Elasticity tensor components C_{ij}

We calculated all single-crystal elasticity tensor components, C_{ij}, with the method of Le Page and Saxe [39, 40]. This method uses the stresses computed in VASP as inputs to a least squares fit of the C_{ij}, treated as unknowns in the linear stress–strain relationships, for a sequence of symmetry-unique strains. The total number of unknown (independent) C_{ij} is three for fcc LiH, six for tetragonal $LiNH_2$, and nine for orthorhombic Li_2NH. Tests were conducted to determine the total number of strains necessary to minimize the least squares errors for each C_{ij}. Strains of 0.3%, 0.4%, 0.5%, 0.6%, 0.7%, and 0.8% were found adequate to obtain $\leqslant$1% statistical error in each computed C_{ij}. The small residuals indicate that anharmonic effects, due to the applied strains, on the computed elastic constants are negligible. Tests with additional intermediate strains showed no significant deviation from the results reported herein. Separate calculations with different **k**-point meshes were also conducted to determine the meshes needed to converge each C_{ij} to $\leqslant$0.5 GPa. All C_{ij} computations were performed on the primitive cell of each distorted structure and employed the same DFT convergence criteria as the structural relaxations on the undistorted structures.

4.4. Elastic stability

4.4.1. Born stability criteria. Since the pioneering work of Born on elastic stability (sometimes referred to as mechanical stability), there has been considerable interest in applying the eponymous 'Born stability criteria' to various crystalline materials (theoretical groundwork can be found in [41]). These criteria, which are conditions on the elastic constants, themselves intrinsic material properties, were originally delineated by Born through expansion of the internal energy in terms of strains followed by a convexity argument for the internal energy. For a crystalline system to be elastically stable, the change in its internal energy, ΔU, due to a homogeneous elastic distortion must be positive definite: $\Delta U > 0$. In the present context, the internal energy is the electronic energy acquired from VASP. Well-known examples of elastic instabilities are the various Bain paths associated with fcc to bcc lattice transformations [31].

The Born criteria must be modified when a crystal is subject to a hydrostatic pressure, P [42, 43]. Since we are specifically interested in the effect of P on the elastic stability of crystalline systems, we employed the methodology in [43]. This provides the following generalization of the elastic constants portion of the Hessian matrix, **H**, due to P:

$$H = \begin{bmatrix} \tilde{C}_{11} & \tilde{C}_{12} & \tilde{C}_{13} & 2C_{14} & 2C_{15} & 2C_{16} \\ \tilde{C}_{21} & \tilde{C}_{22} & \tilde{C}_{23} & 2C_{24} & 2C_{25} & 2C_{26} \\ \tilde{C}_{31} & \tilde{C}_{32} & \tilde{C}_{33} & 2C_{34} & 2C_{35} & 2C_{36} \\ 2C_{41} & 2C_{42} & 2C_{43} & 4\tilde{C}_{44} & 4C_{45} & 4C_{46} \\ 2C_{51} & 2C_{52} & 2C_{53} & 4C_{54} & 4\tilde{C}_{55} & 4C_{56} \\ 2C_{61} & 2C_{62} & 2C_{63} & 4C_{64} & 4C_{65} & 4\tilde{C}_{66} \end{bmatrix}, \tag{7}$$

where

$$\tilde{C}_{kk} = C_{kk} - P(k = 1, \ldots, 6), \qquad \tilde{C}_{12} = C_{12} + P, \qquad \tilde{C}_{13} = C_{13} + P, \quad \text{and} \quad \tilde{C}_{23} = C_{23} + P. \tag{8}$$

Note that the C_{ij} result from our VASP-optimized electronic energies, and the $\tilde{C}_{ij}$ are the pressure-corrected components of the Hessian matrix. The $\tilde{C}_{ij}$ should not be construed as pressure-corrected elastic constants, a fact that can be confirmed through thermodynamic arguments [44]. The eigenvalue condition is

$$|\mathbf{H} - \mathbf{E}| = 0, \tag{9}$$

with **E** the (diagonal) eigenvalue matrix.

The square root of each eigenvalue is a normal mode frequency. A negative eigenvalue implies that the accompanying distortion leads to $\Delta U < 0$ (or enthalpy, if a pressure is applied), leading to elastic and hence thermodynamic instability [45]. Alternatively, relationships exist between the C_{ij} (or linear combinations of the C_{ij}) and the sound velocities (along specific directions) in the crystal [46], with the sound velocities directly related to the slopes of the acoustic phonon branches at low **q** [47]; zero or imaginary velocities signal instability in a manner equivalent to negative eigenvalues of equation (9).

4.4.2. Eigenvalues E_{ii}. We note that analytic expressions exist for the eigenvalues E_{ii} of equation (9) for cubic, tetragonal, and orthorhombic structures, against which our numerical results can be checked. In particular, for the cubic [fcc ($Fm\bar{3}m$)] LiH structure:

$$E_{11} = \tilde{C}_{11} + 2\tilde{C}_{12} \tag{10}$$

$$E_{22} = E_{33} = \tilde{C}_{11} - \tilde{C}_{12} \tag{11}$$

$$E_{44} = E_{55} = E_{66} = 4\tilde{C}_{44}. \tag{12}$$

For tetragonal [$I\bar{4}$] $LiNH_2$:

$$E_{11} = \tilde{C}_{11} - \tilde{C}_{12} \tag{13}$$

$$E_{22}, E_{33} = \tfrac{1}{2}\Big(\tilde{C}_{11} + \tilde{C}_{12} + \tilde{C}_{33} \mp \sqrt{\tilde{C}_{11}^2 + 2\tilde{C}_{11}\tilde{C}_{12} + \tilde{C}_{12}^2 + 8\tilde{C}_{13}^2 - 2\tilde{C}_{11}\tilde{C}_{33} - 2\tilde{C}_{12}\tilde{C}_{33} + \tilde{C}_{33}^2}\Big) \tag{14}$$

$$E_{44}, E_{55}, E_{66} = 4\tilde{C}_{44}, 4\tilde{C}_{44}, 4\tilde{C}_{66}. \tag{15}$$

Algebraic expressions can also be derived for orthorhombic lattices (these are unavailable in the literature), but are too unwieldy to report here.

Table 1. Lattice constant, a, and C_{ij} at selected P for LiH obtained from VASP optimization of the experimental structure ($a = 4.08$ Å [35]). P and C_{ij} in GPa.

P	a (Å)	C_{11}	C_{12}	C_{44}
0	4.02	72.9	10.5	46.0
50	3.34	406.1	58.5	81.7
75	3.21	546.4	83.9	89.4
100	3.11	670.0	108.8	94.5

Table 2. E_{ii} at selected P for LiH. A negative eigenvalue denotes elastic instability. All quantities in GPa.

P	E_{11}	E_{22}	E_{33}	E_{44}	E_{55}	E_{66}
0	62.5	62.5	93.9	184.0	184.0	184.0
50	247.6	247.6	573.1	126.8	126.8	126.8
75	312.5	312.5	789.2	57.6	57.6	57.6
100	361.2	361.2	987.6	−22.0	−22.0	−22.0

4.5. Computed C_{ij} and E_{ii}

Table 1 shows our computed lattice constants, a, and elasticity tensor components, C_{ij}, for LiH at $P = 0$, 50, 75, and 100 GPa. The $Fm\bar{3}m$ space group required three distortions per strain, leading to two structures with $I4/mmm$ and one structure with $Immm$ symmetry. A total of 18 VASP geometry optimizations (three for each of the six selected strains) was required to compute the elastic constants. The **k**-meshes we utilized consisted of 2176 **k**-points in the irreducible Brillouin zone (IBZ) of the $I4/mmm$ structures and 4096 **k**-points in the IBZ of the $Immm$ structure. We note that our C_{11}, C_{12}, and C_{44} values at $P = 0$ agree well with values of 74.1, 13.4 and 48.4 GPa, respectively, from extrapolation of higher temperature experimental data to 0 K in [48].

Table 2 lists our computed E_{ii} for LiH at the same pressures. We predict LiH to be elastically unstable at 100 GPa since three negative E_{ii} are calculated. Existing experimental data suggests that LiH transitions to a metallic B2 (CsCl) structure at 313 GPa, but recent theoretical results suggest a transition to a semiconducting phase at 100 GPa [49]. This is in contrast to the other alkali hydrides [50, 51] where charge transfer from the alkali ion to hydrogen at higher pressures is thought to induce structural instability [52].

Our computed lattice constants a and C_{ij} for $LiNH_2$ and Li_2NH are listed in table 3 at selected P. Differences in the $P = 0$ lattice constants reported in table 3 relative to earlier work [28] are due to the use of PBE PAW potentials in the present work. The tetragonal $I\bar{4}$ space group of $LiNH_2$ mandated six distinct distortions, leading to strained structures with space group symmetries $C2$, $I\bar{4}$, and $P1$. The **k**-meshes used for these structures contained 100 ($C2$), 54 ($I\bar{4}$), and 172 (P1) points in the IBZ. Thirty-six geometry optimizations were necessary to derive the C_{ij} for $LiNH_2$. The orthorhombic $Ima2$ space group of Li_2NH required nine distinct distortions resulting in strained structures with $Ima2$, Cm, Cc, and $C2$ space groups. The **k**-meshes we employed comprised 64 ($Ima2$) and 100 ($Cm, Cc, C2$) **k**-points in the IBZ. Calculation of the nine independent elastic constants for Li_2NH with the chosen strain set necessitated 54 geometry optimizations. We see that $(C_{ii})_{Li_2NH} > (C_{ii})_{LiNH_2}$ for $i = 1, 3, 4$; however, the same trend is not followed by the off-diagonal elastic constants since $(C_{12})_{Li_2NH} < (C_{12})_{LiNH_2}$ at 25 GPa and $(C_{13})_{Li_2NH} < (C_{13})_{LiNH_2}$ at 10 GPa. Li_2NH has a greater resistance to shear distortion than $LiNH_2$ except at 25 GPa where $(C_{66})_{Li_2NH} < (C_{66})_{LiNH_2}$.

Table 4 shows the E_{ii} computed for $LiNH_2$ and Li_2NH based on the C_{ij} in table 3. We note that $LiNH_2$ is elastically unstable at 50 GPa since E_{11}, E_{44}, and $E_{55} < 0$. Li_2NH is elastically unstable at the smaller pressure of 25 GPa since $E_{22} < 0$.

Table 3. Lattice constants a, b, c, and C_{ij} at selected P for $I\bar{4}$ $LiNH_2$ and $Ima2$ Li_2NH from VASP optimization of the experimental structures ($a = 5.04$ Å, $c = 10.28$ Å for $LiNH_2$ [36, 37]; $a = c = 7.13$ Å, $b = 10.09$ Å for Li_2NH [28]). P and C_{ij} in GPa.

Hydride	P	a (Å)	b (Å)	c (Å)	C_{11}	C_{12}	C_{13}	C_{22}	C_{23}	C_{33}	C_{44}	C_{55}	C_{66}
$LiNH_2$	0	5.04	—	10.40	44.0	14.2	16.0	—	—	43.5	14.3	—	20.1
	10	4.59	—	9.82	90.8	41.9	51.3	—	—	105.0	20.8	—	34.5
	25	4.30	—	9.42	154.7	91.8	91.0	—	—	178.3	25.6	—	55.4
	50	4.05	—	8.97	249.2	172.7	155.9	—	—	274.2	25.7	—	83.2
Li_2NH	0	7.15	10.12	7.12	97.6	27.5	20.0	74.4	35.0	87.4	37.0	26.3	32.1
	10	6.81	9.60	6.79	156.6	72.6	39.7	120.3	68.9	164.4	64.5	35.8	72.4
	25	6.51	6.52	9.16	250.2	69.0	114.0	219.9	135.1	169.9	98.9	87.8	47.2

Table 4. E_{ii} at selected P for $LiNH_2$ and $Ima2$ Li_2NH. A negative eigenvalue denotes elastic instability. All quantities in GPa.

Hydride	P	E_{11}	E_{22}	E_{33}	E_{44}	E_{55}	E_{66}
$LiNH_2$	0	30.6	27.3	75.2	57.2	57.2	80.4
	10	28.9	25.1	202.6	43.2	43.2	98.0
	25	12.0	29.4	370.4	2.4	2.4	232.8
	50	−23.5	15.5	630.6	−97.2	−97.2	132.8
Li_2NH	0	141.6	43.5	74.3	148.0	105.2	128.4
	10	278.0	32.2	101.1	218.0	103.2	249.6
	25	450.5	−5.1	119.6	295.6	251.2	88.8

Table 5. Energetics of selected Li_2NH structures in the GGA. Quantities are defined in the text. All energies in kJ mol^{-1} f.u.$^{-1}$ (f.u. ≡ formula unit).

Li_2NH structure	Space group	E_{el}	ΔE_{el}	ZPE	E_0	ΔE_0	δF_{298}	F_{298}	ΔF_{298}
1	$Ima2$[a]	−1698.84	0.00	46.38	−1652.46	0.00	−7.03	−1659.49	0.00
2	$Pnma$[b]	−1699.93	−1.09	46.62	−1653.31	−0.85	−6.57	−1659.88	−0.39
3	$C2/m$[c]	−1701.22	−2.38	46.32	−1654.90	−2.44	−5.56	−1660.46	−0.97
4	$Pnma$[d]	−1701.82	−2.98	47.06	−1654.76	−2.30	−6.16	−1660.92	−1.43
5	$Pbca$[e]	−1703.37	−4.53	46.51	−1656.86	−4.40	−6.47	−1663.33	−3.84

[a] Reference [28].
[b] This work; see table 6.
[c] This work; see table 7.
[d] Reference [29].
[e] Reference [30].

Table 6. Li_2NH $Pnma$ variant of $Ima2$ structure [28]. $a = 7.22$ Å, $b = 7.03$ Å, $c = 10.26$ Å.

Site	Wyckoff position	x	y	z
H	8d	0.510 74	0.393 12	0.805 00
H2	4c	0.166 49	0.250 00	0.550 73
H3	4c	0.837 78	0.250 00	0.515 10
Li	8d	0.743 94	0.537 93	0.860 76
Li2	8d	0.250 77	0.480 72	0.868 69
Li3	4c	0.477 91	0.250 00	0.637 57
Li4	4c	0.559 23	0.250 00	0.142 39
Li5	4c	0.473 05	0.250 00	0.354 64
Li6	4a	0.000 00	0.000 00	0.000 00
N	8d	0.493 84	0.510 53	0.745 21
N2	4c	0.279 13	0.250 00	0.488 38
N3	4c	0.695 51	0.250 00	0.498 45

Table 7. Li_2NH $C2/m$ layered structure. $a = 6.18$ Å, $b = 3.57$ Å, $c = 13.36$ Å, $\alpha = \gamma = 90°$, $\beta = 84.3°$.

Site	Wyckoff position	x	y	z
H	4i	0.991 52	1.000 00	0.926 69
H2	4i	0.592 45	1.000 00	0.433 03
Li	4i	0.671 03	0.000 00	0.876 12
Li2	4i	0.726 73	1.000 00	0.617 54
Li3	4i	0.957 99	0.000 00	0.300 94
Li4	4i	0.644 98	1.000 00	0.205 50
N	4i	0.010 14	1.000 00	0.848 57
N2	4i	0.614 10	1.000 00	0.354 91

4.6. Comparison of Li_2NH structure energetics

The energetics of some additional Li_2NH structures are compared with those of the $Ima2$ structure [28] in table 5. Structures 2 and 3, with the $Pnma$ (orthorhombic) and $C2/m$ (monoclinic) space groups are detailed in tables 6 and 7. Structure 2 is a variant of the $Ima2$ structure with a slightly distorted Li framework, while structure 3 consists of H-terminated layers constructed from a cubic motif with the N–H groups aligned normal to the layers. Structures 4 ($Pnma$) [29] and 5 ($Pbca$) [30] were derived in theoretical work by other authors. In table 5 E_{el} is the total electronic energy; $\Delta E_{el} = E_{el} - E_{el}$ ($Ima2$) is E_{el} of a given structure relative to that of the $Ima2$ structure; ZPE the zero-point energy; $E_0 = E_{el} + ZPE$; $\Delta E_0 = E_0 - E_0$ ($Ima2$); $\delta F_{298} = E_{ph}(T) - TS$ at $T = 298$ K, where E_{ph} is the phonon energy without the ZPE and S is the vibrational entropy; $F_{298} = E_0 + \delta F_{298}$, and $\Delta F_{298} = F_{298} - F_{298}$ ($Ima2$). The structures are listed according to decreasing E_{el}. Thermal expansion effects are neglected. Following [28], all energetics were computed with the hardest GGA (PW91) PAW potentials with each structure fully optimized with comparably dense **k**-point meshes. We note that the −1.09 to −4.53 kJ mol^{-1} f.u.$^{-1}$ range of ΔE_{el} is quite small, with the range of ΔF_{298} at 298 K even smaller. The E_0 for the $C2/m$ layered structure is slightly less than that for the $Pnma$ structure #4, but entropy reverses this at 298 K.

The thermodynamic functions in table 5 were computed from phonon calculations using the direct method (detailed in [19]). Computed vibrational properties of structure 1 may be found in [28]. In all cases, longitudinal optical/transverse optical splittings and the volume dependence of the ZPE were neglected since they have no significant effect on the energies listed in table 5 (see [19] for further discussion of these issues for hydrides). Phonon calculations for structures 2–5 involved 2 × 1 × 1 (128 atom), 1 × 1 × 2 (64 atom), 2 × 2 × 2 (128 atom) and 2 × 2 × 2 (128 atom) supercells, respectively. Phonon dispersion relations and total phonon density of states (DOS) are shown for structures 2, 3, 4, and 5 in figures 3, 4, 5, and 6, respectively. Figures 3(a), 4(a), 5(a), and 6(a) contain 192, 48, 48, and 96 branches, respectively. The absence of soft modes in figures 3–6 suggests that the corresponding structures have stable local energy minima according to DFT. The phonon DOS show some similar characteristics and some obvious differences. For example, each contains one or more high frequency bands corresponding to H vibrational modes; however, structures 3–5 do not feature the two distinct high frequency peaks found in the phonon DOS of the $Ima2$ structure [28] (and in structure #2) which are in close accord with experiment [53, 54]. Each phonon DOS displays a group of low frequencies ranging from 0 to 25 THz. Figure 6(b) shows a small isolated peak at 23 THz in the $Pbca$ phonon DOS that is absent in the other structures.

Despite the fact that the relative energies at 0 and 298 K in table 5 suggest otherwise, we believe that the $Ima2$ structure for crystalline Li_2NH is the most accurate representation (i.e., in best accord with available experimental information) for

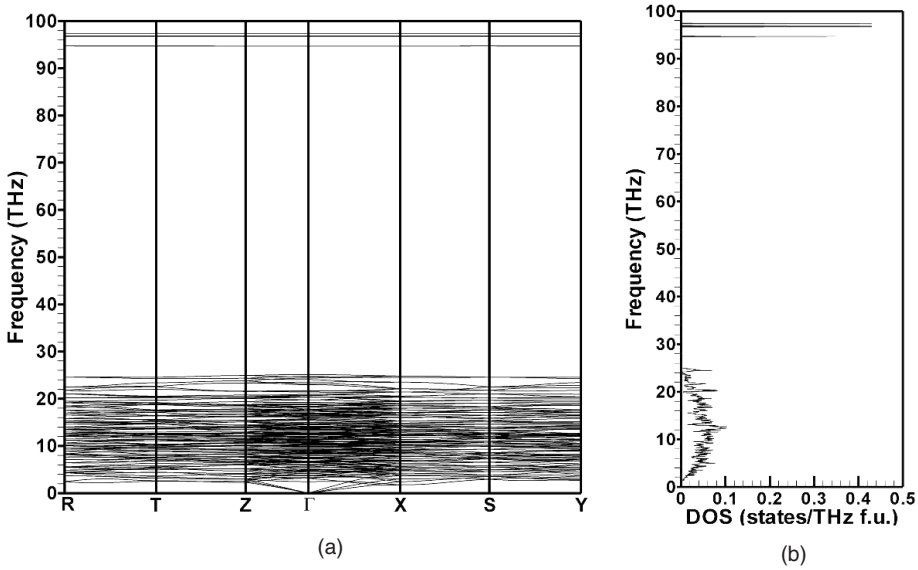

Figure 3. Computed phonon dispersion curves (a) and total phonon density of states (b) for the Li_2NH *Pnma* structure #2 (a variant of the *Ima*2 structure of [28]) in table 5.

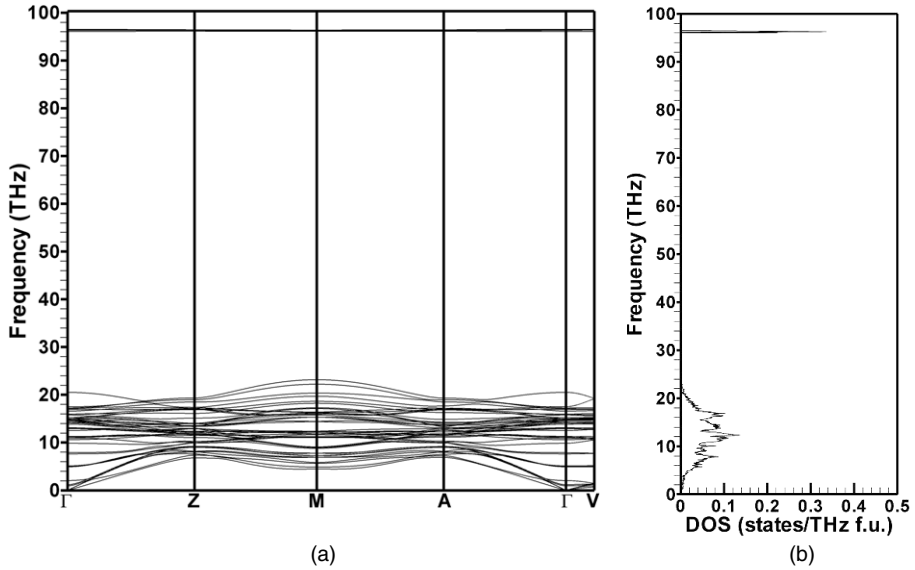

Figure 4. Computed phonon dispersion curves (a) and total phonon density of states (b) for the $C2/m$ Li_2NH structure #3 in table 5.

a number of reasons. First, of the models in table 5, the *Ima*2 structure most closely accommodates the diffraction data in [27]: significant differences in computed diffraction patterns (not reported here) for structures 2–5 suggest that it would be very difficult, if not impossible, to fit these to the experimental data. Second, the measurements in [27], conducted above 50 K on a deuterated sample, showed no evidence of a low temperature phase transition. Rather, an order–disorder transition was observed at 360 K. Third, the phonon DOS derived for the *Ima*2 structure are in best accord with the observed infrared and Raman spectra [53, 54], as we noted above. Fourth, the ΔF_{298} trend in table 5 is contrary to experiment. We would expect $\Delta F_{298} > 0$ for structures 2–5 since none is observed at room temperature in [27]. Although DFT predicts structures 2–5 to be lower in energy than the *Ima*2 structure, we believe that this may be due to intrinsic errors in DFT in general and GGA in particular. Although we cannot fully rule out kinetic effects, distinct structures that are stable at very low temperatures, or errors in the experiment, we believe that these are unlikely causes. The computed structures do strongly suggest the possibility of several different Li_2NH polymorphs that do not differ significantly in energy from the observed low temperature Li_2NH structure [27]. While low energy paths between any of the structures in table 5 have not been determined, each may be important either in substituted compounds or in alternate reaction pathways. Finally, while the issue of structure prediction by theoretical means is of great intrinsic importance,

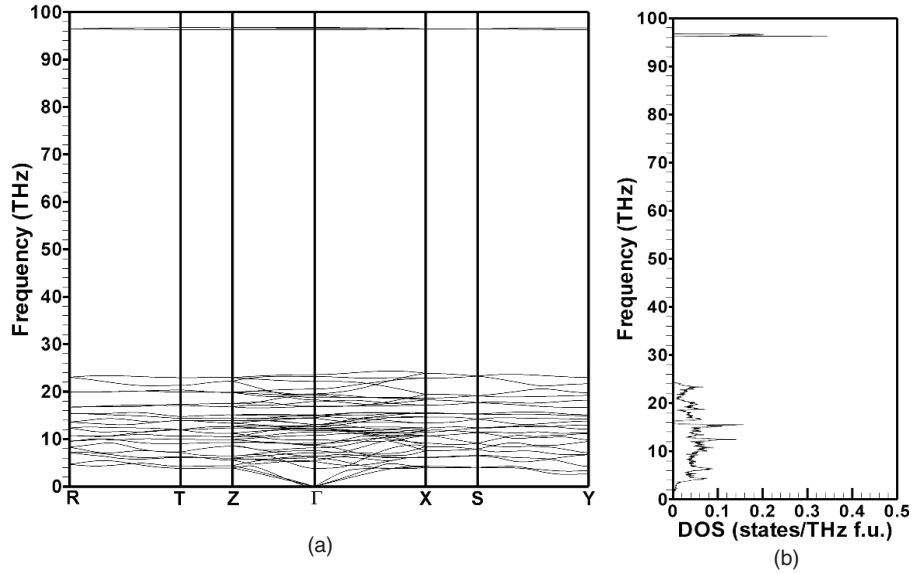

Figure 5. Computed phonon dispersion curves (a) and total phonon density of states (b) for the *Pnma* Li_2NH structure #4 in table 5 [29].

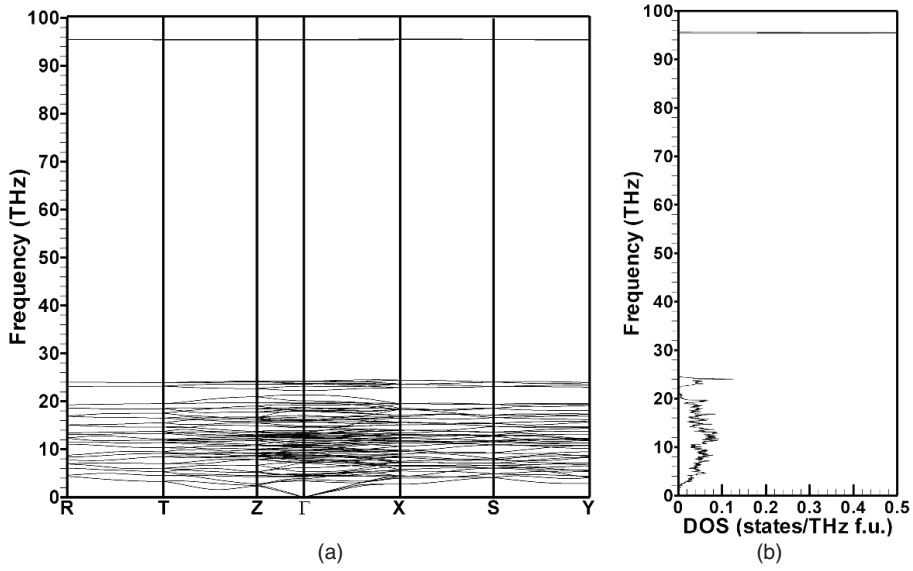

Figure 6. Computed phonon dispersion curves (a) and total phonon density of states (b) for the *Pbca* Li_2NH structure #5 in table 5 [30].

and new methods based upon genetic algorithms [55–57] hold great promise, DFT calculations continue to rely upon accurate structure determination from experiment. While Li_2NH structures derived from inference, database searches, or by other theoretical methods are intriguing, they will ultimately require experimental corroboration.

5. $Li_4BN_3H_{10}$

Pinkerton *et al* [58] reacted 2:1 molar mixtures of $LiNH_2$ and $LiBH_4$ and discovered a new quaternary hydride initially identified as $Li_3BN_2H_8$. This phase is stable at 298 K with respect to $LiNH_2$ and $LiBH_4$, melts at 190 °C, and releases 11 mass% H_2 from the liquid. Filinchuk *et al* [59] subsequently established that the phase is bcc ($I2_13$ space group) and has the precise stoichiometry $Li_4BN_3H_{10}$. This structure was subsequently confirmed by Chater *et al* [60]. Our phonon dispersion relations and density of states computed on the $1 \times 1 \times 1$ conventional cell containing 144 atoms are shown in figures 7(a) and (b), respectively. Tests with larger supercells revealed no significant differences. The phonon dispersion plot contains 216 branches. These results suggest no soft modes in $Li_4BN_3H_{10}$. Computed components of the elasticity tensor are: $C_{11} = 30.6$, $C_{12} = 10.7$, and $C_{44} = 12.6$ GPa (no experimental values are available). The eigenvalues of the stability matrix are all positive definite and hence in agreement with the behavior of the phonon branches at the zone center in figure 7(a).

Using DFT in the GGA (PW91) and a new polymorph for Li_3BN_2 [61], we previously examined four decomposition

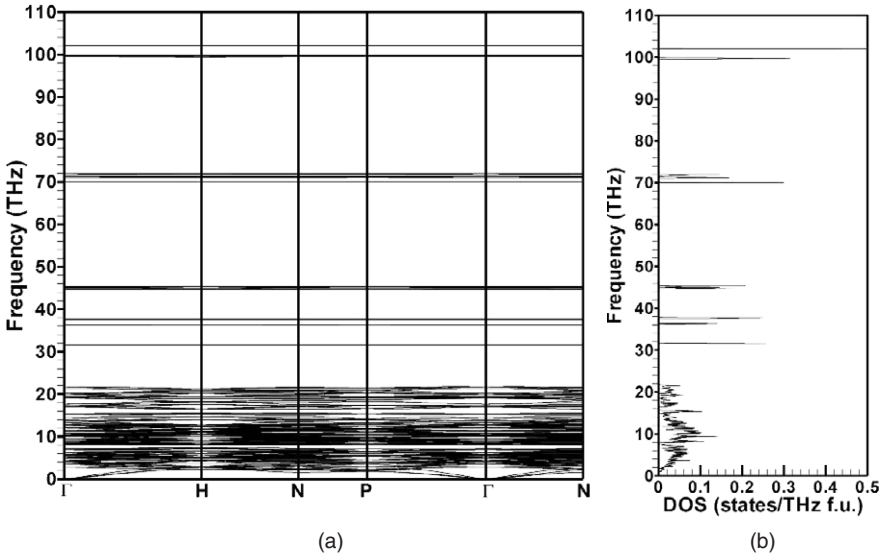

Figure 7. Computed phonon dispersion (a) and total phonon density of states curves (b) for $Li_4BN_3H_{10}$.

pathways for $Li_4BN_3H_{10}$ [62]. Our calculations suggest that

$$Li_4BN_3H_{10} \rightarrow Li_3BN_2 + LiNH_2 + 4H_2 \qquad (16)$$

has the lowest heat of reaction (45 kJ mol^{-1} $Li_4BN_3H_{10}$). On the other hand,

$$Li_4BN_3H_{10} \rightarrow Li_3BN_2 + \tfrac{1}{2}Li_2NH + \tfrac{1}{2}NH_3 + 4H_2 \qquad (17)$$

with a 96 kJ mol^{-1} $Li_4BN_3H_{10}$ heat of reaction is in closest accord with experiment [63]. Siegel *et al* [64] confirmed these essential conclusions. This disagreement between theory and experiment is currently unresolved. A combination of both DFT inaccuracy and more complex reaction mechanisms may be responsible and requires further inquiry on both fronts.

6. Low temperature structures for $LaCo_5$

Vibrational properties of $La(TM)_5$ (TM = Co, Ni) were recently computed in [65]. While vibrational spectra for $LaNi_5$ and $LaNi_5H_7$ revealed no soft modes in either compound at 0 K, the same was not true for $LaCo_5$ and $LaCo_5H_4$ (both ferromagnetic). Of particular interest here is $LaCo_5$, the parent compound of $LaCo_5H_4$, which is a $CaCu_5$-type structure with the $P6/mmm$ space group. The computed phonon dispersion plot (using $2 \times 2 \times 2$ supercells) is shown in figure 8. Slopes of the three branches on either side of the Γ-point are positive. This suggests that $P6/mmm$ $LaCo_5$ is stable against symmetry-unique elastic distortions of the cell. Evaluation of equation (9) with the VASP-computed elastic constants reported in [66] confirms this since six positive eigenvalues result. However, there are several phonon branches in the negative frequency range (negative frequencies are representative of imaginary frequencies): these suggest that the lattice is unstable. In [65] we explored the two modes at the A-point in the IBZ. The vibrations associated with these modes, which correspond to frequencies of −3.157 and −3.158 THz, respectively, and fall within the black open

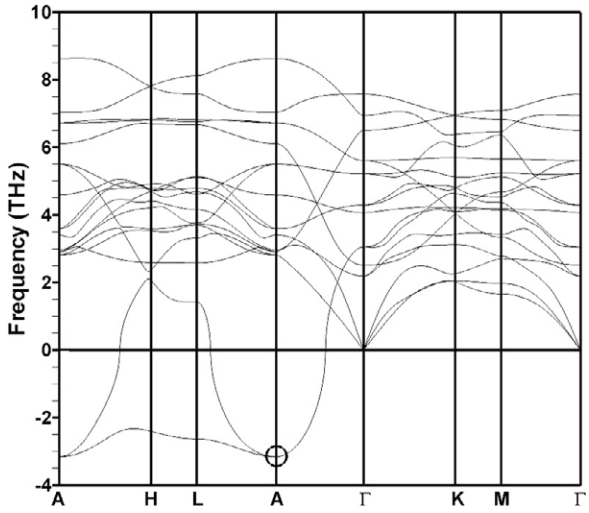

Figure 8. Computed phonon dispersion curves for $P6/mmm$ $LaCo_5$ $2 \times 2 \times 2$ supercell. Open circle at A (0 0 1/2) denotes two imaginary frequencies (represented as negative numbers) at −3.157 and −3.158 THz. The vibrations associated with these soft modes lead to supercell structures with the $Cmmm$ and $Cccm$ space groups.

circle in figure 8, lead to supercell structures with $Cccm$ and $Cmmm$ space groups. Upon optimization, the $Cccm$ structure (reported in [65]) was found to be a stable local energy minimum inasmuch as it features (i) a total electronic energy slightly more negative than that of the $P6/mmm$ structure, (ii) a negative enthalpy of formation ΔH with respect to the elemental metals as well, (iii) elastic constants demonstrating elastic stability by the Born criteria, and (iv) a phonon spectrum with no soft modes. The same is true for the $Cmmm$ structure. These results suggest that a $LaCo_5$ phase exists at low temperature. The picture from experiment tells a different story since $LaCo_5$ undergoes a eutectoid decomposition below ∼600 °C [67]. Hence, there is no known $LaCo_5$ structure at

0 K. This is yet another interesting, and unresolved, divergence between theory and experiment.

7. Conclusions

There is no question whatsoever that DFT has become an extremely valuable tool for the investigation of hydrogen storage materials. Efficient solution of the Kohn–Sham equations with a computational engine such as VASP [2, 3] enables not only the calculation of electronic attributes, but also the derivation of vibrational and elastic properties via powerful auxiliary methods such as those of [12] and [39, 40], respectively. In this paper we have described application of those techniques to predict the elastic constants of LiH, $LiNH_2$, and Li_2NH and to calculate the phonon spectra of various Li_2NH structures, the novel hydride $Li_4BN_3H_{10}$, and $LaCo_5$.

While the capability for generating these kinds of results from first principles is extraordinary, we point out that there are issues regarding accuracy, i.e., comparison with experiment, that remain to be confronted, among them the following. First, the choice of ε_{xc} from the approximations currently available can produce significant variation in quantities such as the enthalpy of formation, as we described for the alkaline earth metals and their hydrides. This makes for uncertainty in selecting ε_{xc} for multicomponent materials (e.g., those containing Mg) for which different ε_{xc} yield more accurate results for the individual constituents. Second, caution must be exercised when inferring an actual crystal structure from 0 K electronic energies E_{el} alone. As we emphasized in the case of lithium imide, many hypothetical structures may feature E_{el} values in close proximity, and definitive identification still requires appeal to experiment in view of the intrinsic uncertainties in the DFT energies, introduced primarily by the approximate nature of ε_{xc}. A third, corollary, implication from our work on $LaCo_5$ is that DFT may suggest a stable zero temperature structure that experiment indicates does not exist. These issues are particularly crucial if the great potential for DFT to guide the discovery of new materials and mechanisms for hydrogen storage, as well as other purposes, is to be realized.

Acknowledgments

The authors are grateful to G P Meisner, F E Pinkerton, P Saxe, E Wimmer, G Kresse, and W Wolf for illuminating discussions.

References

[1] Kohn W and Sham L 1965 *Phys. Rev.* **140** A1133
[2] Kresse G and Hafner J 1994 *Phys. Rev.* B **49** 14251
[3] Kresse G and Furthmüller J 1996 *Comput. Mater. Sci.* **6** 15
[4] Blöchl P E 1994 *Phys. Rev.* B **50** 17953
[5] Kresse G and Joubert D 1999 *Phys. Rev.* B **59** 1758
[6] Ceperley D M and Alder B J 1980 *Phys. Rev. Lett.* **45** 566
[7] Perdew J P and Zunger A 1981 *Phys. Rev.* B **23** 5048
[8] Perdew J P and Wang Y 1992 *Phys. Rev.* B **45** 13244
[9] Perdew J P, Chevary J A, Vosko S H, Jackson K A, Pederson M R, Singh D J and Fiolhais C 1992 *Phys. Rev.* B **46** 6671
[10] Perdew J P, Burke K and Ernzerhof M 1996 *Phys. Rev. Lett.* **77** 3865
[11] Vosko S H, Wilk L and Nusair M 1980 *Can. J. Phys.* **58** 1200
[12] Parliński K 2005 *Software Phonon, Cracow (2001) as implemented in MedeA 2.2, Materials Design, Angel Fire, New Mexico*
[13] Song Y, Guo Z X and Yang R 2004 *Phys. Rev.* B **69** 094205
[14] Liang G, Huot J, Boily S, Van Neste A and Schulz R 1999 *J. Alloys Compounds* **292** 247
[15] Chen D, Wang Y M, Chen L, Liu S, Ma C X and Wang L B 2004 *Acta Mater.* **52** 521
[16] de Castro J F R, Yavari A R, LeMoulec A, Ishikawa T T and Botta W J 2005 *J. Alloys Compounds* **389** 270
[17] Vajo J J, Mertens F, Ahn C C, Bowman R C Jr and Fultz B J 2004 *Phys. Chem.* B **108** 13977
[18] Zaluska A, Zaluski L and Ström-Olsen J O 1999 *J. Alloys Compounds* **289** 197
[19] Hector L G Jr, Herbst J F, Wolf W, Saxe P and Kresse G 2007 *Phys. Rev.* B **76** 014121
[20] Wolverton C, Ozolins V and Asta M 2004 *Phys. Rev.* B **69** 144109
[21] Smithson H, Marianetti C A, Morgan D, Van der Ven A, Predith A and Ceder G 2002 *Phys. Rev.* B **66** 144107
[22] Chen P, Xiong Z, Luo J, Lin J and Tan K L 2002 *Nature* **420** 302
[23] Chen P, Xiong Z, Luo J, Lin J and Tan K L 2003 *J. Phys. Chem.* B **107** 10967
[24] Ichikawa T, Isobe S, Hanada N and Fujii H 2004 *J. Alloys Compounds* **365** 271
[25] Meisner G P, Pinkerton F E, Meyer M S, Balogh M P and Kundrat M D 2005 *J. Alloys Compounds* **404–406** 24
[26] Luo W 2004 *J. Alloys Compounds* **381** 284
[27] Balogh M P, Jones C Y, Herbst J F, Hector L G Jr. and Kundrat M 2006 *J. Alloys Compounds* **420** 326
[28] Herbst J F and Hector L G Jr 2005 *Phys. Rev.* B **72** 125120
[29] Magyari-Köpe B, Ozoliņš V and Wolverton C 2006 *Phys. Rev.* B **73** 220101
[30] Mueller T and Ceder G 2006 *Phys. Rev.* B **74** 134104
[31] Grimvall G 1999 *Thermophysical Properties of Materials* (New York: North-Holland)
[32] Hirth J P and Loethe J 1982 *Theory of Dislocations* 2nd edn (Malabar, FL: Krieger)
[33] Zhou Z and Joós B 1996 *Phys. Rev.* B **54** 3841
[34] Bereznitsky M, Ode A, Hightower J E, Yeheskel O, Jacob I and Leisure R G 2002 *J. Appl. Phys.* **91** 5010
[35] Smith D K and Leider H R 1968 *J. Appl. Crystallogr.* **1** 246
[36] Jacobs H and Juza R 1972 *Z. Anorg. Allg. Chem.* **391** 271
[37] Nagib M and Jacobs H 1973 *Atomkernenergie* **21** 275
[38] Schultz-Coulon V, Irran E M, Putz B and Schnick W 1999 *Z. Anorg. Allg. Chem.* **625** 1086
[39] Le Page Y and Saxe P 2002 *Phys. Rev.* B **65** 104104
[40] Le Page Y, Saxe P and Rodgers J R 2002 *Phys. Status Solidi* **229** 1155
[41] Born M and Huang H 1954 *Dynamical Theory of Crystal Lattices* (Oxford: Clarendon)
[42] Wang J, Li J, Yip S, Phillpot S and Wolf D 1995 *Phys. Rev.* B **52** 12627
[43] Sink'ko G V and Smirnov N A 2002 *J. Phys.: Condens. Matter* **14** 2989
[44] Neumann S and Cohen R E 2004 *J. Phys.: Condens. Matter* **16** 8783
[45] Yip S, Li J, Tang M and Wang J 2001 *J. Mater. Sci. Eng.* A **317** 236
[46] Ledbetter H M 1980 *J. Phys. D: Appl. Phys.* **13** 1879
[47] Goldman V V, Horton G K and Klein M L 1971 *Phys. Rev.* B **4** 567
[48] James B W and Kheyrandish H 1982 *J. Phys. C: Solid State Phys.* **15** 6321
[49] Wang Y, Ahuja R and Johansson B 2003 *Phys. Status Solidi* **235** 370

[50] Duclos S J, Vohra Y K, Ruoff A L, Filipek S and Baranowski B 1987 *Phys. Rev.* B **36** 7664
[51] Ahuja R, Eriksson O, Wills J M and Johansson B J 1988 *J. Phys.: Condens. Matter* **10** L153
[52] Zhang J, Zhang L, Cui T, Li Y, He Z, Ma Y and Zou G 2007 *Phys. Rev.* B **75** 104115
[53] Kojima Y and Kawai Y 2005 *J. Alloys Compounds* **395** 236
[54] Bohger J P, Essmann R R and Jacobs H 1995 *J. Mol. Struct.* **34** 325
[55] Martonak R, Oganov A R and Glass C W 2007 *Phase Transit.* **80** 277
[56] Glass C W, Oganov A R and Hansen N 2006 *Comput. Phys. Commun.* **175** 713
[57] Oganov A R and Glass C W 2006 *J. Chem. Phys.* **124** 244704
[58] Pinkerton F E, Meisner G P, Meyer M S, Balogh M P and Kundrat M 2005 *J. Phys. Chem.* B **109** 6
[59] Filinchuk Y, Yvon K, Meisner G P, Pinkerton F E and Balogh M P 2006 *Inorg. Chem.* **45** 1433
[60] Chater P A, David W I F, Johnson S R, Edwards P P and Anderson P A 2006 *Chem. Commun.* 2439
[61] Pinkerton F E and Herbst J F 2006 *J. Appl. Phys.* **99** 113523
[62] Herbst J F and Hector L G Jr 2006 *Appl. Phys. Lett.* **88** 231904
[63] Meisner G P, Scullin M L, Balogh M P, Pinkerton F E and Meyer M S 2006 *J. Phys. Chem.* B **110** 4186
[64] Siegel D J, Wolverton C and Ozolins V 2007 *Phys. Rev.* B **75** 014101
[65] Herbst J F and Hector L G Jr 2007 *J. Alloys Compounds* **446/447** 188
[66] Hector L G Jr and Herbst J F 2004 *J. Alloys Compounds* **370/1–2** 41
[67] Buschow K H J 1972 *J. Less-Common Met.* **29** 283